# Ultrahigh Storage and Fast Diffusion of Na and K in Blue Phosphorene Anodes

Sankha Mukherjee,[†,§] Lance Kavalsky,[†,§] and Chandra Veer Singh*[,†,‡]

[†]Department of Materials Science and Engineering, University of Toronto, 184 College Street, Suite 140, Toronto, Ontario M5S 3E4, Canada

[‡]Department of Mechanical and Industrial Engineering, University of Toronto, 5 King's College Road, Toronto M5S 3G8, Canada

S Supporting Information

ABSTRACT: In the wake of blue phosphorene's (BP) computational discovery and experimental realization, it has emerged as a versatile material with interesting optical, electrical, and mechanical properties. In this study, using first principles density functional theory calculations, we have investigated the adsorption and diffusion of Na and K over monolayer BP to assess its suitability as Na-ion and K-ion battery anodes. The optimized adsorption energies were found to be −0.96 eV for Na and −1.54 eV for K, which are sufficiently large to ensure stability and safety during operation. In addition, BP could adsorb Na and K atoms up to a stoichiometric ratio of 1:1 which yields a high storage capacity of 865 mA h/g for both adatom species. Through examination of the electronic structure and projected density of states of BP as a function of Na/K concentration, we predict that the band gap of the system increasingly shrinks, and in the case of maximum K adsorption, the band gap diminishes completely. Additionally, the diffusion of Na and K over BP is observed to be ultrafast, especially for K, and anisotropic with modest energy barriers of 0.11 and 0.093 eV for Na and K, respectively. Building upon these findings, we employed vibrational analysis techniques with transition state theory to incorporate kinetic effects and predicted a diffusivity of 7.2×10^{-5} cm^2/s for Na and 8.58×10^{-5} cm^2/s for K on BP. Given these advantages, that is, ultrahigh capacity, electrical conductivity, and high Na/K diffusivity, we conclude that BP can be considered as an excellent candidate for anodes in Na- and K-ion batteries.

KEYWORDS: Na/K ion battery, density functional theory, specific capacity, transition state theory, blue phosphorene, adsorption and diffusion
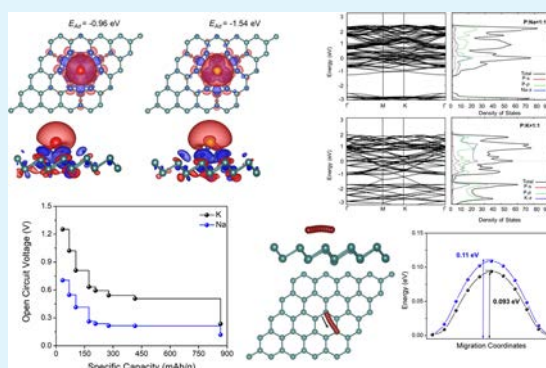
1. INTRODUCTION

Rechargeable lithium-ion batteries (LIBs) have increasingly captured the attention of the energy storage industry in the last two decades because of their extraordinary energy density. Recently, the world's largest Li-ion battery (100 MW) was constructed by Tesla Inc. in Australia which can provide power for up to 30 000 houses when fully charged for 1 h.[1] However, the future use of LIBs is limited, particularly in these large-scale energy storage applications, because of increasing costs of extraction and finite availability of Li. Therefore, as the global reserves for Li continues to drain out, next-generation storage technology will rely on other metal-ion battery devices that are low cost and composed of earth-abundant materials. Potential candidates to replace LIBs that address these drawbacks are sodium (Na)-ion and potassium (K)-ion batteries. The amount of Na and K in earth's crust is 28 400 and 25 900 mg/kg, respectively, whereas the amount of Li stored is only 20 mg/kg.[2] Although the electrochemistries of LIBs, Na-ion batteries (NIBs), and K-ion batteries (KIBs) are similar, the latter two provide several advantages beyond their material abundance including: (a) Na is softer than Li and can therefore suppress

dendrite formation, which is a problem for LIBs.[3] (b) The standard potential for the K+/K system is −2.88 V compared to a standard potential of −2.79 eV for Li+/Li ions. Thus, K-ion batteries can be beneficial in applications requiring higher voltages.[4] (c) Aluminum, which is cheaper than copper, does not alloy with either Na or K, so it can be implemented as a low-cost alternative current collector in NIBs and KIBs,[5,6] unlike LIBs wherein costly copper current-collectors are used. Moreover, the electrolyte solutions and salts used in KIBs (e.g., KPF$_6$) are cheaper and easy to produce.[7] However, despite these benefits neither NIBs nor KIBs have reached the specific capacities of LIBs in general because of the larger effective radii increasing interaction among the Na and K atoms.[8] The greater size of Na and K ions relative to Li presents additional considerations for electrode stability and cyclability (arising from increased strain under intercalation) that need to be addressed to achieve practicality.[6,9] While the inferiority of

NIBs and KIBs relative to LIBs in this regard may hinder their ability to directly replace LIBs in the portable electronics market, the low cost of Na and K gives them the opportunity to replace them in the stationary energy storage market.[5]

The performance of metal-ion batteries predominantly depends on the material properties of the anodes which impacts safety and cycling life. Therefore, searching for advanced materials with large storage capacity and ultrafast charging/discharging rates is key to the success of future battery technologies. Over the past few decades, lack of development of anode materials for NIBs and KIBs has largely been due to the exemplary success story of LIBs. However, when transitioning away from LIBs, anode materials that are suitable for LIBs may not be appropriate for NIBs and KIBs. The root of this hindrance is the differences in potential and atomic radii of Li, Na, and K. For example, graphite, which is commercially used for intercalating of Li ions in LIBs, struggles to intercalate Na[10] because of the energetically unstable intercalation compounds of Na and graphite[11] which leads to poor storage capacity.[12]

Because high performing anode materials for LIBs do not necessarily translate well to NIBs and KIBs, much work has been conducted to identify suitable anode materials for these novel battery technologies.[7,9] For two-dimensional (2D) NIB anodes, graphene, various transition metal oxides, MXenes, and transition metal dichalcogenides have all been considered.[9] On the other hand, for anodes in KIBs, much emphasis has been placed on carbon-based anodes, especially graphite, which produces stable intercalation compounds but suffers from poor cyclability.[5,6] In this context, 2D materials and their heterostructures are appealing because of their large surface to volume ratios and excellent electronic, thermal, and mechanical properties. For example, alkali metal-ion batteries (AIBs) made of 2D materials of group IV elements such as graphene[13,14] and borophene[15,16] have been investigated because of their excellent electrochemical performance as battery electrodes. For another group V element, phosphorus, theoretical investigations so far have reported more than 15 2D polymorphs, with black and blue phosphorene being of interest. First principles studies have found black phosphorus to be a material with ultrahigh storage capacity and high charging/discharging rates for metal-ion batteries,[17,18] and experimentally, black phosphorus/graphene hybrids have demonstrated desirable parameters as well for LIBs and NIBs. Alternatively, blue phosphorene (BP), theoretically predicted in 2014,[19] has a puckered surface similar to the structure of silicene, has somewhat flatter "zigzag" edges than the "armchair" edges found in black phosphorene, and should provide more space for the diffusion of the metal ions. The successful synthesis of BP in 2016[20] using epitaxial growth begs the question of whether BP can be effectively used in metal-ion battery applications. First principles investigations have studied the suitability of monolayer BP,[21] BP/graphene, BP/NbS$_2$, and BP/TaS$_2$[22] heterostructures as negative electrodes in LIBs. For example, Li et al.[21] reported that the monolayer BP has a Li storage capacity equal to 865 mA h/g and a Li diffusion barrier of merely 0.16 eV. On the basis of these theoretical estimates, the applicability of pristine monolayer BP as a negative electrode in NIBs and KIBs is worth exploring.

To determine pristine monolayer BP's aptitude for NIBs and KIBs, density functional theory (DFT) calculations were conducted to predict its specific capacity and ionic diffusion barriers. First, favorable sites for the adsorption of the metal ions over BP were identified. To obtain estimates of charge capacity, the adsorption energies of Na and K over BP were estimated as a function of the composition by increasing ion coverage. The open-circuit voltage profiles for different compositions of Na and K were also calculated from the adsorption energy data. Additionally, charge density difference analysis and partial density of states (PDOS) calculations were performed to gain further insight into the adsorption process and to characterize the electronic properties of Na- and K-decorated BP. Climbing image-nudged elastic band (CI-NEB) simulations were employed to determine the minimum energy pathways (MEPs) and the diffusion energy barriers for transport of the metal atoms over BP. Additionally, vibrational analysis was conducted, and diffusivities of Na and K over BP were calculated following the principles of transition state theory. The results presented in this manuscript demonstrate that monolayer BP is well-suited as a negative electrode for next-generation NIBs and KIBs.

2. COMPUTATIONAL METHODS

Plane wave-based DFT simulations were performed using the Perdew–Burke–Ernzerhof[23] exchange–correlation functional within the generalized gradient approximation through the Quantum ESPRESSO package.[24] While Troullier–Martins norm-conserving pseudopotentials[25] were used for the electronic structure, phonon dispersion, adsorption energy, and energy barrier calculations, projected augmented wave (PAW) pseudopotentials were used for the Bader charge analysis.[26] The atomic positions and lattice constants of monolayer BP were calculated using a kinetic energy cutoff of 60 Ry for the wave functions and 480 Ry for charge density computations. The convergence threshold of the self-consistent field method was set to 1×10^{-6} Ry. A vacuum spacing of 20 Å was used above the BP surface to avoid interactions arising from van der Waal's forces between BP layers and metal adatoms. The unit cell of freestanding monolayer BP was optimized using a conjugate gradient minimization over a $13 \times 13 \times 3$ Monkhorst–Pack[27] grid of k-points with the residual Hellmann–Feynman force on each atom less than 0.001 Ry per bohr, and the total energy converged within 0.0001 Ry. The optimization of the BP supercell and binding energy simulations were performed over a $4 \times 4 \times 1$ Monkhorst–Pack[27] grid of k-points. For postprocessing analysis, all of the structures were visualized with XCrysden[28] and VESTA.[29] The pristine BP supercell consisted of 5×5 unit cells (with 50 atoms). The dispersion corrections arising from van der Waals forces were taken into account by employing the DFT-D2 approach.[30] Previous research has demonstrated that the DFT-D2 approach provides results with reasonable accuracy in adsorption energies and diffusional energy barriers for Li–graphite structures.[31] The optimized adsorption positions were calculated by placing the alkali metal atoms above the P atoms at different sites, followed by relaxation. The adsorption energy (E_{Ad}) and charge density difference (ρ_{Ad}) were determined by

$$E_{Ad} = E_{adsorbed\,state} - (E_{adsorbent} + E_{substrate}) \qquad (1)$$

$$\rho_{Ad} = \rho_{adsorbed\,state} - (\rho_{adsorbent} + \rho_{substrate}) \qquad (2)$$

where $E_{adsorbed\,state}$ is the energy of BP after the adsorption of Na/K, $E_{adsorbent}$ is the energy of a Na/K atom in their body centered cubic bulk form, and $E_{substrate}$ is the energy of monolayer BP. A negative E_{Ad} indicates that adsorption is favored, and more negative values of E_{Ad} imply stronger binding. Hereafter, we use the terms "adsorption" and "binding" interchangeably. Likewise, $\rho_{adsorbed\,state}$ is the charge density of BP after the adsorption of Na/K, $\rho_{adsorbent}$ is the charge density of an isolated Na/K atoms, and $\rho_{substrate}$ is the charge density of monolayer BP. For commercial purposes, the average adsorption energy (E_{avg}) and open circuit voltage (OCV) are widely used for characterizing the performance of alkaline batteries, such as the state-of-charge and battery health. E_{avg} and OCV can be evaluated by estimating the voltage for a range of metal atom stoichiometry. E_{avg} is given by
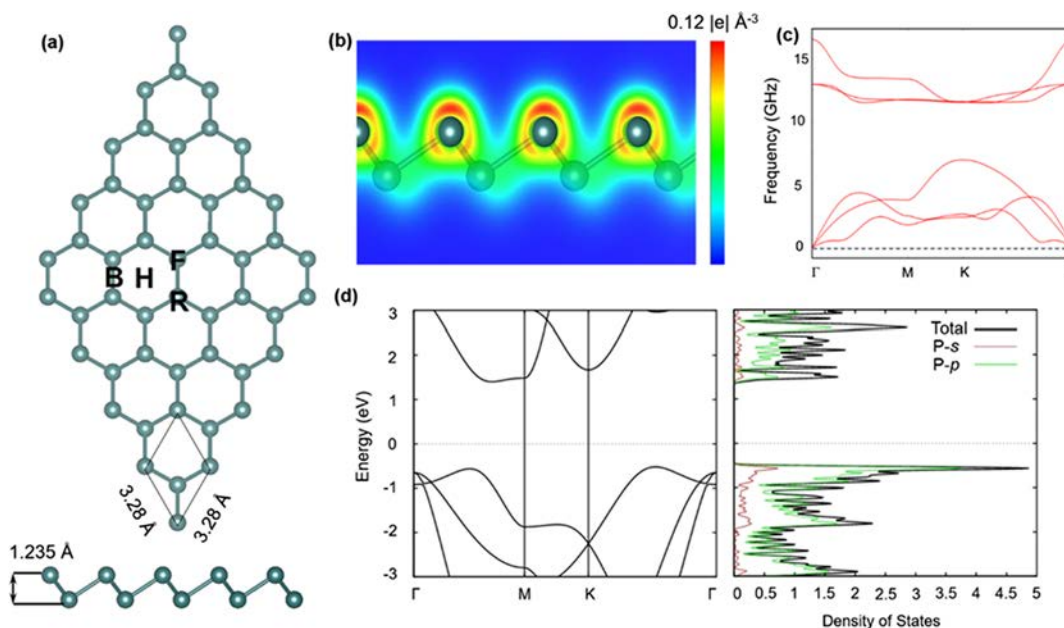
Figure 1. (a) Top view and side view of the unit cell of BP. The unit cell is shown by black rhombus. (b) Valence electron density. Different colors represent distinct levels of electron density. (c) Phonon dispersion in BP. (d) Band structure and partial density of states of BP at the ground state.

$$E_{avg} = \frac{E_{adsorbed\ state} - n \times E_{adsorbent} - E_{substrate}}{n} \quad (3)$$

where n is the number of Na/K atoms adsorbed. For computation of the density of states plots, Gaussian smearing was applied. The degauss value was selected by balancing accuracy with the ability to reflect bonding characteristics of the system. For our simulations, we chose a width of 0.0025 Ry.

The voltage profile of the secondary battery is an important aspect because it is closely related to the total energy storage of the battery. As shown in previous works, this parameter may be estimated using the following relation under the assumption that PV and TS are negligible[22,32−34]

$$OCV \approx \frac{-E_{avg}}{e} \quad (4)$$

where e is the elementary charge, and a positive value of OCV implies favorable adsorption. In comparison to adsorption energy, we take negative values as being favorable. The storage capacity of BP can be calculated using Faraday's equation, given by

$$q = 1000 \times F \times z \frac{n}{M_{BP}} \quad (5)$$

where F, n, M_{BP}, and z are Faraday's constant (26.801 A·h/mol), number of metal atoms adsorbed over BP, mass of BP, and number of valence electrons involved in the electrochemical process. The CI-NEB method was used to find estimates of energy barriers for the diffusion of Na/K over BP.[35]

The stability of pristine BP was confirmed through computation of the phonon dispersion curve employing the phonopy[36] package where no imaginary frequencies were observed. Additionally, variable cell ab initio molecular dynamics (AIMD) was employed to evaluate the thermodynamical stability of double-sided adsorption. Velocity rescaling algorithm was used to maintain the temperature at 300 K with a time step of 2 fs for relaxation.

To calculate the kinetic rate constant for the diffusion reaction, the Eyring equation[37] was employed

$$k = \frac{k_B T}{h} e^{-\Delta G_A / k_B T} \quad (6)$$

where k_B is the Boltzmann constant, T is the temperature, h is Planck's constant, and ΔG_A is the Gibbs free energy of activation. Using order

of magnitude arguments to eliminate $P\Delta V$,[38] the Gibbs free energy of activation becomes

$$\Delta G_A = E_a + \Delta ZPE - T\Delta S \quad (7)$$

with E_a representing the activation energy found from CI-NEB, ΔZPE is the change in the zero-point energy, and $T\Delta S$ is the change in entropy between the initial state and the transition state. The entropy consists of a configurational component and a vibrational component, but the former is taken to be negligible[39] leaving only the vibrational component to be considered. This leads to eq 7 taking the approximate form of

$$\Delta G_A \cong E_a + \Delta F_{vib} \quad (8)$$

where ΔF_{vib} is the change in the vibrational Helmholtz free energy and is defined as the change in vibrational entropy subtracted from the change in zero-point energy. The substrate was also fixed under the approximation that the substrate has minimal vibrations, as done previously.[40] With these approximations in mind, ΔF_{vib} was calculated using the built-in Quantum ESPRESSO interface of Atomic Simulation Environment[41] to determine the vibrational modes of the adatom through the finite displacement method in the harmonic limit. The vibrational Helmholtz free energy was calculated using the formula

$$F_{vib} = \sum_i \frac{\hbar \omega_i}{2} + k_B T \ln\left(1 - \exp\left[\frac{-\hbar \omega_i}{k_B T}\right]\right) \quad (9)$$

where $\hbar$ is the reduced Planck's constant and ω_i is the i-th vibrational frequency of the adatom. This method displaces the adatom (in our case 0.01 Å) in the ± direction of each Cartesian direction and calculates the difference in energies to approximate the Hessian matrix. For these SCF computations to determine the displaced energies, only gamma was considered for Brillouin zone sampling which is consistent with previous reports.[42,43]

Building upon the kinetic rate constant, the diffusivity of each adatom on BP may be determined through the transition state theory relation[44]

$$D = \lambda^2 k \quad (10)$$

where λ is the distance between adjacent stable sites.
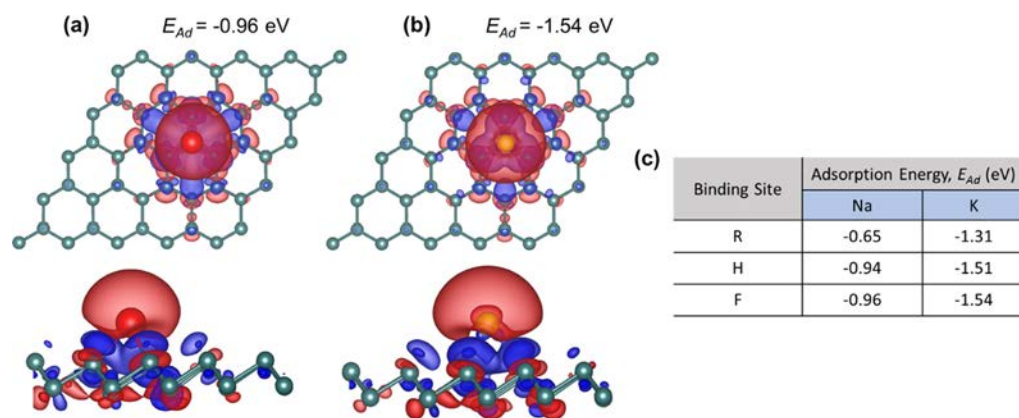
Figure 2. Top view and side view of charge density difference plots for the most stable adsorption sites for (a) Na and (b) K over BP. Color code for atoms: green, P; red, Na; and yellow, K. The isosurface level is set to be 0.0005 eÅ^{-3}. Blue and light red regions indicate charge accumulation and depletion, respectively. (c) Adsorption energies for Na/K over three different adsorption sites in BP.
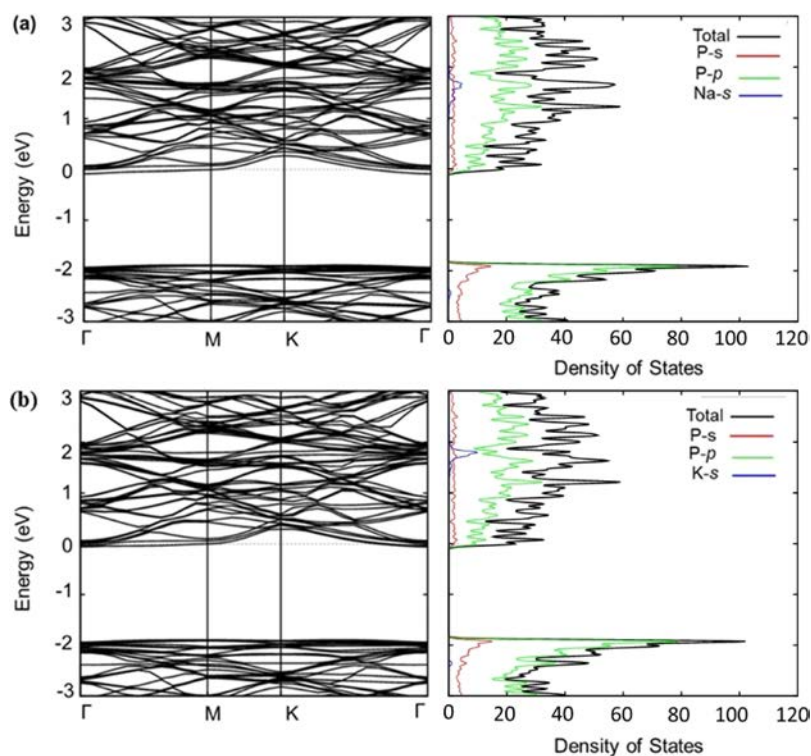
Figure 3. Band structure (left) and PDOS (right) of BP with (a) one Na adatom and (b) one K adatom.

3. RESULTS AND DISCUSSION

3.1. Electronic and Structural Properties of BP. The optimized structure of a freestanding monolayer BP supercell and valence electron densities are shown in Figure 1a. As revealed in this figure, BP has a puckered structure, and as a result, the P atoms belong to two atomic planes along its thickness, unlike its group IV cousin graphene. In Figure 1a, the BP unit cell is bordered using black lines with corresponding lattice constants, $a_1 = a_2 = 3.28$ Å, which agree with previous reports (3.28,[45] 3.268 Å[22]). Each P atom is covalently bonded with three P neighbors, having a P−P bond length of 2.26 Å and a bond angle of 93°. Figure 1b shows the valence electron density in BP which displays a graphical representation of the locations where electrons in the outermost shell are most likely to reside. Here, an accumulation of charge is observed near the P−P valleys of BP. During the alkali-metal adsorption process,

these electrons are available for bonding purposes. Additionally, the phonon dispersion relation for BP at the ground state is shown in Figure 1c, demonstrating its dynamical stability. Figure 1d displays the band diagram and PDOS of the primitive cell of BP where it has an indirect band gap of ~1.95 eV, which agrees well with previous reports.[46]

3.2. Adsorption of Na and K over BP. For a material to be suitable as an anode in an AIB, it must exhibit a strong binding energy of the metal adatoms. As shown in Figure 1a, four geometrically unique adsorption sites were considered for both Na/K atoms, which are (a) above the center of the P hexagon (H-site), (b) above the P atom in the ridge (R-site), (c) above the center of a P−P bond (B-site), and (d) above the P atom along the furrow (F-site). First, a single metal adatom was placed at 3 Å over the surface of BP, and the system was optimized by minimizing the total ground state energy. The

adsorption energy was calculated using eq 1, and the minimum energy configuration was identified by comparing the adsorption energies of all the sites. For the most energetically favorable configuration, Table S1 presents the distance (r) between Na/K and BP, perpendicular height (h), structural distortion (ΔZ_{max}) of BP, adsorption energy (E_{Ad}) for an H-site, R-site, and F-site. By comparison of adsorption energies, for both Na and K adatoms the F-site is the most favored site with binding energies of −0.96 and −1.54 eV, respectively. The metal adatoms drift over to an F-site when placed above a B-site. Notably, for both Na and K, the adsorption energies of the F-site and H-site are comparable. Negative adsorption energies for a range of adsorption sites indicate that Na and K storage over BP is a spontaneous process and suggest that Na and K atoms prefer adsorption over BP rather than cluster formation, which is of paramount importance for the safety of AIBs.[17] Equilibrium charge density difference contours of Na and K adsorption over an F-site are presented in Figure 2a,b. Evidently, strong ionic Na−P and K−P bonds are formed after adsorption because of the length of the P−P bonds around the metal atom increasing slightly and consequently swelling the hexagonal P ring. Additionally, charge accumulation takes place near the puckered hexagonal ring of BP while charge-depleted regions surround the Na/K atoms, indicating net charge transfer from the metal adatoms to BP. To quantify the amount of charge transfer during the adsorption process, Bader charge analysis was carried out.[26] The results show that over an F-site, while the charged state of a Na atom is +0.894|e|, for a K atom the charge state is +0.926|e| (here, the charge state implies the difference between the valence charge of the isolated metal adatom and its charge after adsorption). Moreover, the effect of vacuum on the adsorption energy of Na and K over an F-site was tested, and the results are presented in Figure S2. It can be seen that the values of E_{Ad} vary by a meager 0.02 eV for Na and 0.05 eV for K for vacuum lengths varying between 10 and 30 Å.

To study the effect of adsorption of Na and K on the system's electronic properties, the PDOS and band structures for each species were calculated. As shown in Figure 3, the Fermi levels in the BP systems containing Na/K adatoms are pulled into the conduction band. Accordingly, much improved conductivity is expected relative to pristine BP in both adsorption cases because of an increase in the number of charge carriers. Upon further examination of the plots, both adatoms mainly contribute s-states in the conduction band above the Fermi energy, thereby implying their donation of electrons to this band via ionic bonding. In other words, the adatoms n-dope the system through the contribution of electron charge carriers. The predicted behavior is highly beneficial to BP's suitability in the proposed context as the aim is to minimize internal resistance to the motion of electrons for maximizing the overall battery performance. As will be addressed in the next section, this behavior is further exaggerated upon multiple adsorption.

3.3. Theoretical Voltage and Capacity. During the charging/discharging process in NIBs/KIBs, the concentration of the metal adatoms changes, thereby affecting the theoretical voltage and storage capacity of the battery. Therefore, it is important to study the thermodynamics of the adsorption process as a function of the alkali atom density. To compute the storage capacity and voltage of BP as a function of Na and K compositions, a 5 × 5 supercell was considered. The adatoms were placed over the F-sites at 3 Å above the substrate for double-sided adsorption, and the systems were relaxed. To

assess the maximum allowable concentration of the adatoms, it has been ensured that the per atom adsorption energy (E_{avg}) for metal atoms are negative. It is also known that during the adsorption process for larger concentrations of metal adatoms, strong interactions between the substrate and adatoms can weaken, or even cause failure, in the resultant structure. These bonds cannot repair with time and the battery ceases to be useful. Therefore, BP cannot suffer irreversible deformation during the adsorption process to be viable in the proposed context. To determine adsorption stability, the method proposed by Tritsaris et al. was employed;[47] wherein, the metal atoms from the fully adsorbed phases are removed, and a new energy minimization is performed on the bare substrate. For the adsorption of Na/K over BP, the structural parameters (e.g., lattice constants, bond angles, and bond lengths) of the final system closely resemble that of pristine BP, indicating a reversible deformation of the substrate during adsorption. Different compositions of Na$_x$P and K$_x$P were studied with x taking on values of 0.04, 0.08, 0.12, 0.2, 0.24, 0.32, 0.48, and 1. The charge density difference plots for the stable structures and the corresponding values of E_{avg} as a function of x are shown in Figure 4a−c. Simulations reveal that as the concentration of the metal adatoms is increased, the electrostatic repulsive force acting among the adatoms gradually increases, hence weakening the subsequent adsorption. The highest Na/K concentration is a 1:1 ratio between the adatoms and P atoms (i.e., NaP and KP), which leads to a specific capacity of 865 mA h/g for both Na and K. The corresponding E_{avg} values are −0.12 and −0.24 eV for Na and K, respectively. When additional adatoms are introduced they are either pushed away from the BP surface or the substrate undergoes irreversible deformation. Upon Na atom intercalation for a concentration of 1:1, the lattice constant of BP increases by 4.45%, by expanding from 3.28 to 3.431 Å. On the other hand, for K intercalation the BP lattice undergoes severe deformation, and the lattice constant increases to 3.85 Å, a growth of 17.3%. This behavior can be attributed to the difference in the atomic radius of Na and K, as the effective radius of Na is only 227 pm compared to 280 pm for K. Moreover, for intercalation of Na (at a 1:1 concentration), the pucker height of BP decreases from 1.6 Å (which is the pucker height of pristine BP) to 1.16 Å; whereas for K intercalation, this width decreases to only 0.81 Å. We conducted AIMD simulations to evaluate dynamic stability of the substrate with double-sided adsorption at a concentration of 1:0.2 (Figure S1). The structure was observed to be stable over the time investigated. The open circuit voltage as a function of specific capacity is shown in Figure 4d. It can be noted that the low values of voltages indicate suitability as an anode material. Additionally, the voltage profile of BP for increasing concentrations of Na and K is similar to that of graphene,[48] 2D MoS$_2$ and VS$_2$ nanocomposites,[49] Ti$_3$C$_2$,[8] and other 2D materials.[16,50]

To further explore the effect of increasing the number of adatoms on the electronic behavior of the system, the band structure and PDOS were recalculated at the maximum concentration of metal adsorption (i.e., with 50 adatoms on 50 P atoms). Starting with Na, as the substrate becomes more populated with adatoms, more states are contributed to the conduction band, further n-doping the system as shown in Figure 5a. This has the effect of pulling the Fermi level even further into the conduction band and increasing the likelihood of vastly improved conductivity. Turning attention to K, significant changes occur, as evidenced in both the PDOS and
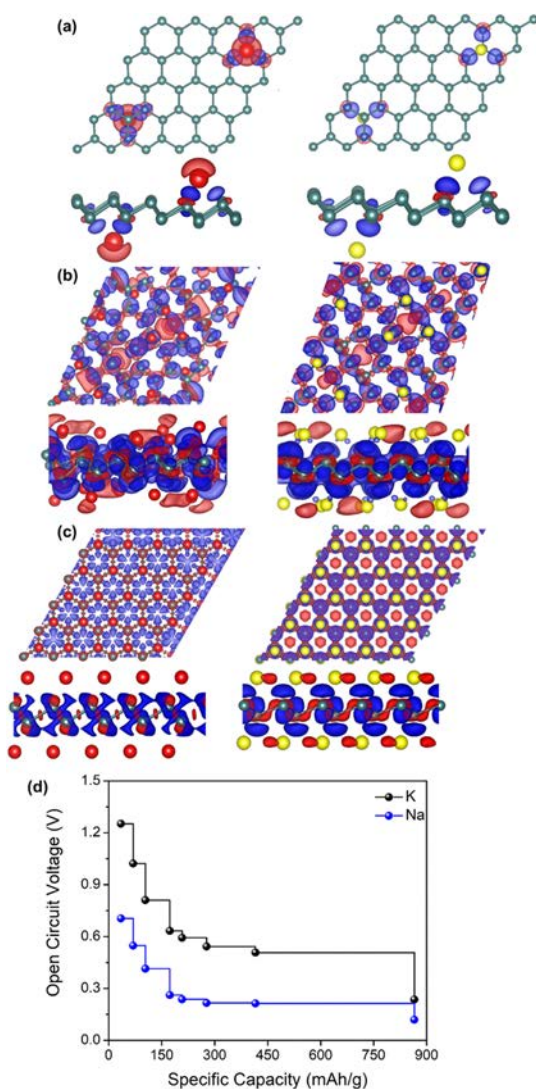
Figure 4. Top view and side view of charge density difference plots for the most stable adsorption sites over BP for (a) 2, (b) 16, and (c) 50 Na/K atoms. Color code for atoms: green, P; red, Na; and yellow, K. The isosurface level is set to be 0.002 eÅ^{-3}. (d) Open-circuit voltage for Na/K adatoms as a function of specific capacity.

band structure plots (Figure 5b), by the destruction of the band gap which implies a semiconductor-to-metallic transition. Furthermore, by examination of the band diagrams, it becomes clear that the transition to a metal is a consequence of the donation of bands that cross the original location of the band gap under the repeated adsorption. Similarly, for the Na case, the PDOS in Figure 5b shows the donation of states above where the Fermi level was, but the distribution shape has also been altered to eliminate the band gap. As a result, conductivity is expected to increase, and metallic behavior is anticipated. In summary, repeated adsorption of either Na or K improves the conductive nature of the system enforcing BP's potential as an anode in either NIBs or KIBs.

3.4. Diffusion Energy Barriers and Diffusivity Coefficient for Na/K Mobility.
The performance of AIBs is determined by the rate of the charging/discharging cycle which relies upon the mobility of the metal atoms over the anode. The mobility of the adatoms is determined by the diffusion barrier associated with the transport of the atom and the electric conductivity of BP, where smaller energy barriers would

facilitate faster diffusion. Poor ionic diffusivity leads to significant structural damage with continued cycling, consequently affecting the lifetime of the battery. Additionally, with increasing concentration of Na/K, the band gap either reduces with the Fermi level being pulled into the conduction band (Figure 5a) or the gap disappears entirely (Figure 5b). Therefore, after Na/K adsorption, electrons are expected to become progressively more mobile in BP.

As discussed earlier, differences in the binding energies of Na/K over F-sites and P-sites are minimal. Therefore, adatoms will diffuse over BP by hopping from either of these two sites to their nearest neighbors. Herein, to find the MEPs for Na/K diffusion, four distinct paths were investigated bearing in mind the structural symmetries inherent to BP. As shown in Figure 6, these MEPs are: (a) path F → R → H → F along the armchair direction, (b) path F → F along the zigzag direction, (c) path H → B → H along the zigzag direction, and (d) path H → F → H along the zigzag direction. The energy profiles associated with these pathways are displayed on the right side of Figure 6.

Considering the path F → R → H → F, the energy barriers for Na and K diffusion are 0.24 and 0.18 eV, respectively. Hopping from an R-site across an H-site to the next F-site during the latter portion of this path requires overcoming a barrier of only 0.054 eV for Na and 0.049 eV for K. However, migration from one F-site to the next R-site, at the beginning of this path, demands a relatively larger barrier to surpass (0.24 eV for Na and 0.18 eV for K). Thus, the R-site acts as a transient state in this case. In comparison, the energy required for diffusing through path F → F is relatively lower for both metal ions. For this path, a transient state appears at the center of the path with energy barriers of 0.11 eV for Na and 0.093 eV for K. On the other hand, diffusion from one H-site to another H-site can occur as either H → B → H or H → F → H. The energy barriers for diffusion over a B-site (path H → B → H) are 0.11 and 0.05 eV for Na and K, respectively. Interestingly, the energy profile associated for the diffusion of both Na/K over an F-site (path H → F → H) are almost identical, and the associated barriers are a meager 0.05 eV in both cases, given that the binding energies are very similar for an F-site versus an H-site. In short, the following can be concluded from the CI-NEB simulations: (I) diffusion of Na and K over BP is anisotropic and diffusion in the zigzag direction is faster than in the armchair direction (reminiscent of the diffusion of Li over black phosphorene,[51] borophene,[52] and unlike silicene[47] and graphene[53]). (II) Overall, the energy barriers corresponding with the diffusion of K are smaller than those for Na which implies that K would diffuse faster than Na on BP.

To achieve a higher level of accuracy regarding the diffusive capabilities of Na and K on BP, vibrational contributions were considered through the Gibbs free energy of activation for diffusion. First, eq 6 allows for the calculation of the kinetic rate constant for the diffusion reactions of both Na and K on BP using the tenets of transition state theory. For each of the transition states, one imaginary vibrational frequency of the adatom was encountered (and excluded from calculations) as expected for a transition state.[43] Without these additional considerations, and only considering the activation energy, the diffusivity through the Eyring equation[37] was calculated to be 9.6×10^{-5} cm^2/s for Na and 1.85×10^{-4} cm^2/s for K. However, the incorporation of the kinetic effects, stemming from zero-point energy and entropy, decreases these values to 7.2×10^{-5} and 8.58×10^{-5} cm^2/s for Na and K, respectively. These results are similar to those for graphite over which both
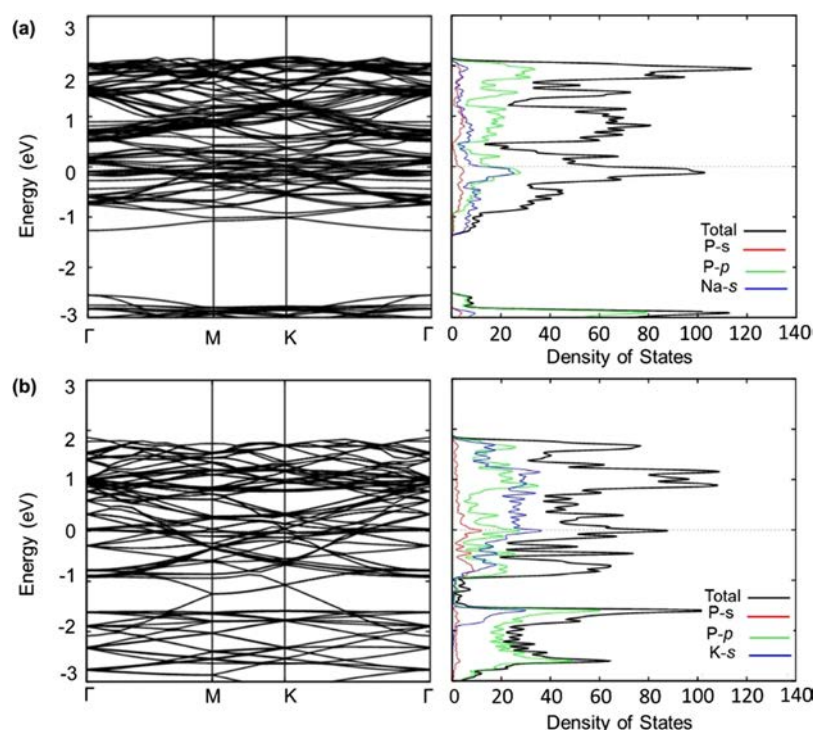
Figure 5. Band structure (left) and PDOS (right) of BP with (a) 50 Na adatoms and (b) 50 K adatoms.

DFT calculations and experiments report a higher diffusivity for K than Na.[54,55] Through experimental investigation of Na diffusivity in hard carbon, it was found to be of order 10^{-9} cm^2/s during most of the sodiation and desodiation processes but reaches as low as 10^{-13} cm^2/s at low voltages.[56] Compared with our predicted value, Na is expected to reach higher diffusivity values of approximately 10^8 times larger in BP than hard carbon. Because of recent experimental advances, researchers managed to measure diffusivity of Li adatoms along the surface of bilayer graphene to be up to 7×10^{-5} cm^2/s at room temperature.[57] Compared with our values for Na and K on BP, this experimental result is of similar magnitude after the incorporation of kinetic effects through vibrational analysis. Diffusivities of Na and K over BP for temperatures between 50 and 500 K are depicted in Figure S2.

3.5. Comparison with Other 2D Anode Materials. Recently, a host of research groups around the world have invested much effort into screening different 2D materials for anodes in AIBs. So far, the selection of simulation techniques (DFT, ab initio MD), choice of pseudopotentials (BHS, PAW, Ultrasoft, norm-conserving), and computational parameters (van der Waals correction, self-consistent field accuracy, energy and force cutoffs, etc.) have been inconsistent in these works. As a result, difficulties arise in making direct comparisons between previously predicted values. However, while the exact values are expected to vary under changing parameters, a rough comparison may be conducted to give a general sense of blue phosphorene's predicted performance relative to existing 2D anode studies for AIBs.

To place the results presented here within the context of other investigated 2D materials for anodes in NIBs and KIBs, a summary of existing works is highlighted in Table 1. For a material to arise as an appropriate candidate in AIBs it must possess a balance of both high specific capacity and low diffusion barriers. Contrasting the diffusivity of BP to

borophene and MoN$_2$ (the smallest and largest energy barriers of previously studied 2D anode materials) by using Arrhenius's equation, $D \approx \exp\left(\frac{-E_a}{k_B T}\right)$, where E_a is the energy barrier, k_B is the Boltzmann's constant, and T is the temperature, allows for its ranking among previous anodes to be established. The diffusivities of metal ions determine the charging/discharging rates of AIBs at finite temperatures. As discussed earlier, D can be calculated from first principles by estimating contributions from both ZPE and TS. However, theoretical and experimental estimates of D for Na/K over various 2D materials are currently missing. Nevertheless, qualitative comparisons can be drawn on the performance of various 2D materials based on the magnitudes of E_a available in the literature. Starting with Na, the diffusivity over BP is approximately 10^7 times greater than that of MoN$_2$[33] and relatively close to that of borophene.[58] Similarly, for K, the diffusivity over BP is approximately 10^6 times larger than MoN$_2$[33] and again only a meager 10^1 times smaller than borophene.[58] The takeaway message from these diffusivity ratios is that while BP does not possess the highest diffusivities, it is closer to the best option for this parameter than many other available choices.

The observed specific capacities provide another tool for which BP may be ranked among other anode options. Regarding this material property, BP demonstrates a predicted specific capacity among the highest for Na and the highest for K. One of the reports places black phosphorene joint highest with BP for Na, and hexagonal BC$_3$ is the second largest for K.[18,59] However, for black phosphorene there is disagreement in the literature regarding its maximum stable adsorption concentration,[17,18] and hexagonal BC$_3$'s diffusion barriers have not yet been explored in this context to our knowledge which limits its current ability to compete in terms of overall performance. MoN$_2$ is the next best available option in terms of specific capacity for Na, but its lackluster diffusion barriers rule
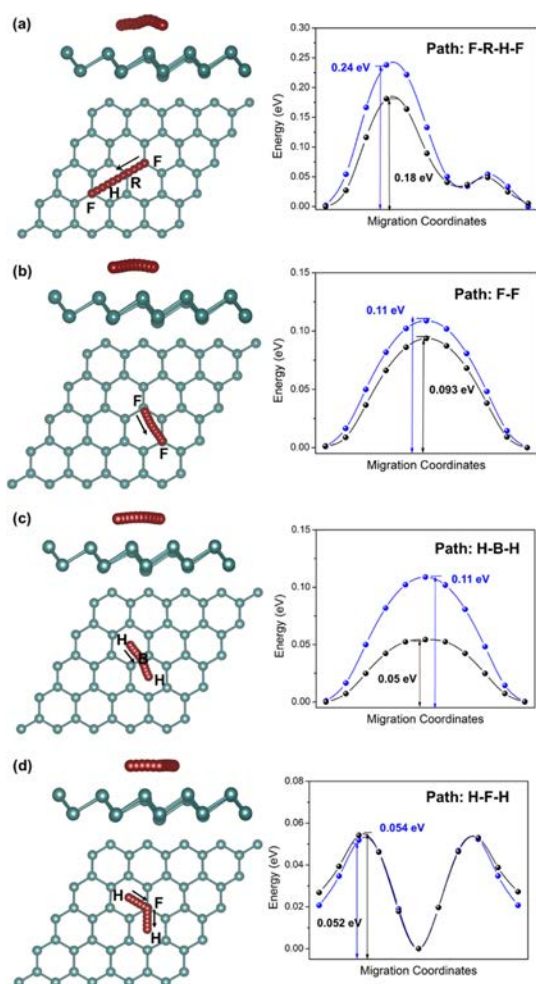
Figure 6. Different diffusional pathways and associated energy barriers for the diffusion of Na and K (black) over pristine BP. (a) Path F → R → H → F along the armchair direction, (b) path F → F along the zigzag direction, (c) path H → B → H along the zigzag direction, and (d) path H → F → H along the zigzag direction. Energy profile associated with the diffusion of Na (blue) and K (black). Black arrows represent the direction of diffusion. Color code for atoms: green, P and brown, Na/K.

it out of contention.[33] The next best available option for K is Ti$_2$CP$_2$, but its capacity is 20% lower than that of BP and also has a larger diffusion barrier.[60]

On the basis of our theoretical predictions and the previous discussion of relative performance, BP provides a solid avenue for future NIB and KIB anode applications because of its overall performance. While BP's diffusion barriers are not to the level of borophene's, they remain respectable when using the previous relative diffusivity arguments, and BP outperforms borophene in terms of charge held. Another competitor for BP in terms of overall performance is VS$_2$; however like borophene, it has inferior specific capacity relative to BP. Plus, the relatively small capacities displayed by V$_2$CP$_2$, Ti$_2$CSi$_2$, and V$_2$CSi$_2$, rule them out despite their comparable diffusions barriers to BP. In summary, when looking for a balance of both large specific capacity and a minimal diffusion barrier, BP emerges as an all-around candidate for both NIBs and KIBs. Even though BP's diffusion barriers are not at the very top of the existing pack, its high specific capacity helps to surpass this deficiency when considering overall predicted performance.

Table 1. Theoretical Performance of Various 2D Anodes for Na/K-Ion Batteries

anode materials	theoretical specific capacity (mA h/g)		diffusion barrier (eV)	
	Na	K	Na	K
blue phosphorene	865	865	0.11	0.093
black phosphorene[17,18]	316	265		0.02
	865		0.04	
borophene[58]	601	397	0.003	0.004
boron phosphide[61]	143	570	0.22	0.16
MoN$_2$[33]	864	432	0.56	0.49
Ti$_3$C$_2$[8]	352	192	0.096	0.10
TiS$_2$[62]	479	479	0.13	0.09
VS$_2$[63,64]	466	466		0.061
	233		0.0085	
2D GeS[65]	256	512	0.09	0.05
SiS[66]	446		0.135	
SiSe[66]	250		0.158	
hexagonal BC$_3$[59]	572	858		
Ti$_2$CP$_2$[60]	711	711	0.3	0.2
V$_2$CP$_2$[60]	610	610	0.13	0.06
Ti$_2$CSi$_2$[60]	327	327	0.22	0.078
V$_2$CSi$_2$[60]	315	236	0.08	0.04
ReS$_2$[67]	428		0.16	

4. CONCLUSIONS

The experimental realization of blue phosphorene, which possesses unique structural, optical, mechanical, and electronic properties, has opened the door for its use in a multitude of applications. Given that the requirements of portable, sustainable, and green energy are increasing more than ever and that LIBs are costly even with their advantages, the question of whether BP can be used as an anode in other AIBs to improve performance was addressed. In this study, using first principles DFT calculations, we have investigated the adsorption and diffusion of Na and K over monolayer BP and thereby evaluated its suitability as NIB and KIB battery anodes. The optimized adsorption energies of Na and K over BP were found to be −0.96 and −1.54 eV, respectively, which are sufficiently large to ensure stability and safety under operating conditions. In addition, monolayer BP could adsorb Na and K atoms up to a stoichiometric ratio of 1:1, resulting in a staggeringly high storage capacity of 865 mA h/g in both cases. Electronic structure calculations (PDOS and band structure) revealed that with increasing concentrations of adatoms, the band gap of the system gradually diminishes, and the Fermi level is pulled out of the gap, most likely increasing the conductivity. Additionally, the diffusion of Na and K over BP was found to be anisotropic with modest energy barriers in the armchair direction of 0.11 and 0.093 eV for Na and K, respectively. By calculating the vibrational modes of the adatoms at the initial and transition states, we predict diffusivity values of 7.2×10^{-5} and 8.58×10^{-5} cm^2/s for Na and K, respectively. These results present many interesting opportunities for developing next-generation anode materials with large capacities, ultrafast charging/discharging rates, and improved efficiencies.

■ ASSOCIATED CONTENT

Ⓢ Supporting Information

The Supporting Information is available free of charge on the ACS Publications website at DOI: 10.1021/acsami.7b18595.

Distance between Na/K and BP and other parameters for an H-site, R-site, and F-site in BP; adsorption energy of Na and K over an F-site for varying vacuum lengths; energy versus time for AIMD for K and Na; and diffusivity of Na and K over BP as a function of temperature (PDF)

■ AUTHOR INFORMATION

Corresponding Author

*E-mail: chandraveer.singh@utoronto.ca.

ORCID Ⓘ

Chandra Veer Singh: 0000-0002-6644-0178

Author Contributions

§S.M. and L.K. contributed equally to the work. All the authors contributed toward preparing the manuscript and have given approval to current version.

Notes

The authors declare no competing financial interest.

■ ACKNOWLEDGMENTS

■ REFERENCES

(1) BBC News Tesla mega-battery in Australia activated. http://www.bbc.com/news/world-australia-42190358 (accessed Dec 1, 2017).

(2) Holleman, A.; Wiberg, N. *Lehrbuch der Anorganischen Chemie*; De Gruyter: Berlin, 2007.

(3) Adelhelm, P.; Hartmann, P.; Bender, C. L.; Busche, M.; Eufinger, C.; Janek, J. From lithium to sodium: cell chemistry of room temperature sodium–air and sodium–sulfur batteries. *Beilstein J. Nanotechnol.* 2015, 6, 1016.

(4) Bie, X.; Kubota, K.; Hosaka, T.; Chihara, K.; Komaba, S. A novel K-ion battery: hexacyanoferrate(II)/graphite cell. *J. Mater. Chem. A* 2017, 5, 4325–4330.

(5) Eftekhari, A.; Jian, Z.; Ji, X. Potassium secondary batteries. *ACS Appl. Mater. Interfaces* 2016, 9, 4404–4419.

(6) Wu, X.; Leonard, D. P.; Ji, X. Emerging Non-Aqueous Potassium-Ion Batteries: Challenges and Opportunities. *Chem. Mater.* 2017, 29, 5031–5042.

(7) Pramudita, J. C.; Sehrawat, D.; Goonetilleke, D.; Sharma, N. An Initial Review of the Status of Electrode Materials for Potassium-Ion Batteries. *Adv. Energy Mater.* 2017, 7, 1602911.

(8) Er, D.; Li, J.; Naguib, M.; Gogotsi, Y.; Shenoy, V. B. Ti3C2 MXene as a high capacity electrode material for metal (Li, Na, K, Ca) ion batteries. *ACS Appl. Mater. Interfaces* 2014, 6, 11173–11179.

(9) Peng, L.; Zhu, Y.; Chen, D.; Ruoff, R. S.; Yu, G. Two-Dimensional Materials for Beyond-Lithium-Ion Batteries. *Adv. Energy Mater.* 2016, 6, 1600025.

(10) DiVincenzo, D. P.; Mele, E. J. Cohesion and structure in stage-1 graphite intercalation compounds. *Phys. Rev. B: Condens. Matter Mater. Phys.* 1985, 32, 2538.

(11) Nobuhara, K.; Nakayama, H.; Nose, M.; Nakanishi, S.; Iba, H. First-principles study of alkali metal-graphite intercalation compounds. *J. Power Sources* 2013, 243, 585–587.

(12) Ge, P.; Fouletier, M. Electrochemical intercalation of sodium in graphite. *Solid State Ionics* 1988, 28, 1172–1175.

(13) Wang, G.; Shen, X.; Yao, J.; Park, J. Graphene nanosheets for enhanced lithium storage in lithium ion batteries. *Carbon* 2009, 47, 2049–2053.

(14) Yang, S.; Li, S.; Tang, S.; Dong, W.; Sun, W.; Shen, D.; Wang, M. Sodium adsorption and intercalation in bilayer graphene from density functional theory calculations. *Theor. Chem. Acc.* 2016, 135, 164.

(15) Jiang, H. R.; Lu, Z.; Wu, M. C.; Ciucci, F.; Zhao, T. S. Borophene: A promising anode material offering high specific capacity and high rate capability for lithium-ion batteries. *Nano Energy* 2016, 23, 97–104.

(16) Rao, D.; Zhang, L.; Meng, Z.; Zhang, X.; Wang, Y.; Qiao, G.; Shen, X.; Xia, H.; Liu, J.; Lu, R. Ultrahigh energy storage and ultrafast ion diffusion in borophene-based anodes for rechargeable metal ion batteries. *J. Mater. Chem. A* 2017, 5, 2328–2338.

(17) Kulish, V. V.; Malyi, O. I.; Persson, C.; Wu, P. Phosphorene as an anode material for Na-ion batteries: a first-principles study. *Phys. Chem. Chem. Phys.* 2015, 17, 13921–13928.

(18) Sibari, A.; Kerrami, Z.; Kara, A.; Hamedoun, M.; Benyoussef, A.; Mounkachi, O.; Benaissa, M. Adsorption and diffusion on a phosphorene monolayer: a DFT study. *J. Solid State Electrochem.* 2017, 22, 11–16.

(19) Zhu, Z.; Tománek, D. Semiconducting layered blue phosphorus: a computational study. *Phys. Rev. Lett.* 2014, 112, 176802.

(20) Zhang, J. L.; Zhao, S.; Han, C.; Wang, Z.; Zhong, S.; Sun, S.; Guo, R.; Zhou, X.; Gu, C. D.; Yuan, K. D.; Li, Z.; Chen, W. Epitaxial growth of single layer blue phosphorus: a new phase of two-dimensional phosphorus. *Nano Lett.* 2016, 16, 4903–4908.

(21) Li, Q.-F.; Duan, C.-G.; Wan, X. G.; Kuo, J.-L. Theoretical prediction of anode materials in Li-ion batteries on layered black and blue phosphorus. *J. Phys. Chem. C* 2015, 119, 8662–8670.

(22) Peng, Q.; Wang, Z.; Sa, B.; Wu, B.; Sun, Z. Blue phosphorene/MS2 (M = Nb, Ta) heterostructures as promising flexible anodes for lithium-ion batteries. *ACS Appl. Mater. Interfaces* 2016, 8, 13449–13457.

(23) Perdew, J. P.; Burke, K.; Ernzerhof, M. Generalized Gradient Approximation Made Simple. *Phys. Rev. Lett.* 1996, 77, 3865–3868.

(24) Giannozzi, P.; Baroni, S.; Bonini, N.; et al. QUANTUM ESPRESSO: a modular and open-source software project for quantum simulations of materials. *J. Phys.: Condens. Matter* 2009, 21, 395502.

(25) Troullier, N.; Martins, J. L. Efficient pseudopotentials for plane-wave calculations. *Phys. Rev. B: Condens. Matter Mater. Phys.* 1991, 43, 1993.

(26) Tang, W.; Sanville, E.; Henkelman, G. A grid-based Bader analysis algorithm without lattice bias. *J. Phys.: Condens. Matter* 2009, 21, 084204.

(27) Monkhorst, H. J.; Pack, J. D. Special points for Brillouin-zone integrations. *Phys. Rev. B: Condens. Matter Mater. Phys.* 1976, 13, 5188–5192.

(28) Kokalj, A. Computer graphics and graphical user interfaces as tools in simulations of matter at the atomic scale. *Comput. Mater. Sci.* 2003, 28, 155–168.

(29) Momma, K.; Izumi, F. VESTA 3 for three-dimensional visualization of crystal, volumetric and morphology data. *J. Appl. Crystallogr.* 2011, 44, 1272–1276.

(30) Barone, V.; Casarin, M.; Forrer, D.; Pavone, M.; Sambi, M.; Vittadini, A. Role and effective treatment of dispersive forces in materials: Polyethylene and graphite crystals as test cases. *J. Comput. Chem.* 2009, 30, 934–939.

(31) Ganesh, P.; Kim, J.; Park, C.; Yoon, M.; Reboredo, F. A.; Kent, P. R. C. Binding and diffusion of lithium in graphite: quantum monte carlo benchmarks and validation of van der Waals density functional methods. *J. Chem. Theory Comput.* 2014, 10, 5318–5323.

(32) Sun, X.; Wang, Z.; Fu, Y. Q. Adsorption and diffusion of sodium on graphene with grain boundaries. *Carbon* 2017, 116, 415–421.

(33) Zhang, X.; Yu, Z.; Wang, S.-S.; Guan, S.; Yang, H. Y.; Yao, Y.; Yang, S. A. Theoretical prediction of MoN2 monolayer as a high capacity electrode material for metal ion batteries. *J. Mater. Chem. A* 2016, 4, 15224–15231.

(34) Wang, D.; Liu, Y.; Meng, X.; Wei, Y.; Zhao, Y.; Pang, Q.; Chen, G. Two-dimensional VS 2 monolayers as potential anode materials for lithium-ion batteries and beyond: first-principles calculations. *J. Mater. Chem. A* 2017, *5*, 21370−21377.

(35) Henkelman, G.; Uberuaga, B. P.; Jónsson, H. A climbing image nudged elastic band method for finding saddle points and minimum energy paths. *J. Chem. Phys.* 2000, *113*, 9901−9904.

(36) Togo, A.; Tanaka, I. First principles phonon calculations in materials science. *Scr. Mater.* 2015, *108*, 1−5.

(37) Eyring, H. The activated complex in chemical reactions. *J. Chem. Phys.* 1935, *3*, 107−115.

(38) Reuter, K.; Scheffler, M. Composition, structure, and stability of $RuO_2(110)$ as a function of oxygen pressure. *Phys. Rev. B: Condens. Matter Mater. Phys.* 2001, *65*, 035406.

(39) Soon, A.; Todorova, M.; Delley, B.; Stampfl, C. Thermodynamic stability and structure of copper oxide surfaces: A first-principles investigation. *Phys. Rev. B: Condens. Matter Mater. Phys.* 2007, *75*, 125420.

(40) Ji, Y.; Dong, H.; Yang, M.; Hou, T.; Li, Y. Monolayer germanium monochalcogenides (GeS/GeSe) as cathode catalysts in nonaqueous Li−O2 batteries. *Phys. Chem. Chem. Phys.* 2017, *19*, 20457−20462.

(41) Larsen, A. H.; Mortensen, J. J.; Blomqvist, J.; Castelli, I. E.; Christensen, R.; Dułak, M.; Friis, J.; Groves, M. N.; Hammer, B.; Hargus, C. The Atomic Simulation Environment—A Python library for working with atoms. *J. Phys.: Condens. Matter* 2017, *29*, 273002.

(42) Miao, M.; Nardelli, M. B.; Wang, Q.; Liu, Y. First principles study of the permeability of graphene to hydrogen atoms. *Phys. Chem. Chem. Phys.* 2013, *15*, 16132−16137.

(43) Huang, L. F.; Ni, M. Y.; Zheng, X. H.; Zhou, W. H.; Li, Y. G.; Zeng, Z. Ab initio simulations of the kinetic properties of the hydrogen monomer on graphene. *J. Phys. Chem. C* 2010, *114*, 22636−22643.

(44) Gulbransen, E. A. The Transition State Theory of the Formation of Thin Oxide Films on Metals. *Trans. Electrochem. Soc.* 1943, *83*, 301−317.

(45) Ding, Y.; Wang, Y. Structural, electronic, and magnetic properties of adatom adsorptions on black and blue phosphorene: a first-principles study. *J. Phys. Chem. C* 2015, *119*, 10610−10622.

(46) Sun, M.; Chou, J.-P.; Yu, J.; Tang, W. Electronic properties of blue phosphorene/graphene and blue phosphorene/graphene-like gallium nitride heterostructures. *Phys. Chem. Chem. Phys.* 2017, *19*, 17324−17330.

(47) Tritsaris, G. A.; Kaxiras, E.; Meng, S.; Wang, E. Adsorption and diffusion of lithium on layered silicon for Li-ion storage. *Nano Lett.* 2013, *13*, 2258−2263.

(48) Zhang, R.; Wu, X.; Yang, J. Blockage of ultrafast and directional diffusion of Li atoms on phosphorene with intrinsic defects. *Nanoscale* 2016, *8*, 4001−4006.

(49) Samad, A.; Shin, Y.-H. MoS2@VS2 nanocomposite as a superior hybrid anode material. *ACS Appl. Mater. Interfaces* 2017, *9*, 29942−29949.

(50) Meng, Q.; Hu, A.; Zhi, C.; Fan, J. Theoretical prediction of MXene-like structured Ti_3C_4 as a high capacity electrode material for Na ion batteries. *Phys. Chem. Chem. Phys.* 2017, *19*, 29106−29113.

(51) Li, W.; Yang, Y.; Zhang, G.; Zhang, Y.-W. Ultrafast and directional diffusion of lithium in phosphorene for high-performance lithium-ion battery. *Nano Lett.* 2015, *15*, 1691−1697.

(52) Jiang, H. R.; Lu, Z.; Wu, M. C.; Ciucci, F.; Zhao, T. S. Borophene: a promising anode material offering high specific capacity and high rate capability for lithium-ion batteries. *Nano Energy* 2016, *23*, 97−104.

(53) Fan, X.; Zheng, W. T.; Kuo, J.-L. Adsorption and diffusion of Li on pristine and defective graphene. *ACS Appl. Mater. Interfaces* 2012, *4*, 2432−2438.

(54) Wang, Z.; Ratvik, A. P.; Grande, T.; Selbach, S. M. Diffusion of alkali metals in the first stage graphite intercalation compounds by vdW-DFT calculations. *RSC Adv.* 2015, *5*, 15985−15992.

(55) Komaba, S.; Hasegawa, T.; Dahbi, M.; Kubota, K. Potassium intercalation into graphite to realize high-voltage/high-power potassium-ion batteries and potassium-ion capacitors. *Electrochem. Commun.* 2015, *60*, 172−175.

(56) Wang, K.; Jin, Y.; Sun, S.; Huang, Y.; Peng, J.; Luo, J.; Zhang, Q.; Qiu, Y.; Fang, C.; Han, J. Low-Cost and High-Performance Hard Carbon Anode Materials for Sodium-Ion Batteries. *ACS Omega* 2017, *2*, 1687−1695.

(57) Kühne, M.; Paolucci, F.; Popovic, J.; Ostrovsky, P. M.; Maier, J.; Smet, J. H. Ultrafast lithium diffusion in bilayer graphene. *Nat. Nanotechnol.* 2017, *12*, 895−900.

(58) Xiang, P.; Chen, X.; Zhang, W.; Li, J.; Xiao, B.; Li, L.; Deng, K. Metallic borophene polytypes as lightweight anode materials for non-lithium-ion batteries. *Phys. Chem. Chem. Phys.* 2017, *19*, 24945−24954.

(59) Joshi, R. P.; Ozdemir, B.; Barone, V.; Peralta, J. E. Hexagonal BC3: A robust electrode material for Li, Na, and K ion batteries. *J. Phys. Chem. Lett.* 2015, *6*, 2728−2732.

(60) Zhu, J.; Schwingenschlögl, U. P and Si functionalized MXenes for metal-ion battery applications. *2D Materials* 2017, *4*, 025073.

(61) Jiang, H. R.; Shyy, W.; Liu, M.; Wei, L.; Wu, M. C.; Zhao, T. S. Boron phosphide monolayer as a potential anode material for alkali metal-based batteries. *J. Mater. Chem. A* 2017, *5*, 672−679.

(62) Samad, A.; Shafique, A.; Shin, Y.-H. Adsorption and diffusion of mono, di, and trivalent ions on two-dimensional TiS2. *Nanotechnology* 2017, *28*, 175401.

(63) Wang, D.; Liu, Y.; Meng, X.; Wei, Y.; Zhao, Y.; Pang, Q.; Chen, G. Two-dimensional VS2 Monolayers as Potential Anode Materials for Lithium-ion Batteries and Beyond: First-Principles Calculations. *J. Mater. Chem. A* 2017, *5*, 21370−21377.

(64) Putungan, D. B.; Lin, S.-H.; Kuo, J.-L. Metallic VS2 Monolayer Polytypes as Potential Sodium-Ion Battery Anode via ab Initio Random Structure Searching. *ACS Appl. Mater. Interfaces* 2016, *8*, 18754−18762.

(65) Li, F.; Qu, Y.; Zhao, M. Germanium sulfide nanosheet: a universal anode material for alkali metal ion batteries. *J. Mater. Chem. A* 2016, *4*, 8905−8912.

(66) Jiang, H.; Zhao, T.; Ren, Y.; Zhang, R.; Wu, M. Ab initio prediction and characterization of phosphorene-like SiS and SiSe as anode materials for sodium-ion batteries. *Sci. Bull.* 2017, *62*, 572−578.

(67) Mukherjee, S.; Banwait, A.; Grixti, S.; Koratkar, N.; Singh, C. V. Adsorption and Diffusion of Lithium and Sodium on Defective Rhenium Disulfide: A First Principles Study. *ACS Appl. Mater. Interfaces* 2018, *10*, 5373−5384.